(Received 23 May 2025, Accepted 1 July 2025, Scheduled 19 July 2025)

No Weighting Factor PMSM Model Predictive Torque Control Based on Composite Sliding Mode Disturbance Observer

Yang Zhang[1], Chenhui Liu[1], Sicheng Li[1], Kun Cao[1], Yiping Yang[1], and Zhun Cheng[2,*]

[1]*Hunan University of Technology, Zhuzhou 412007, China*
[2]*Hunan Railway Professional Technology College, Zhuzhou 412001, China*

ABSTRACT: To address the problems of difficulty in adjusting weight coefficients in model predictive torque control of permanent magnet synchronous motors and the large influence of parameters on the motor control performance, a no weighing factor model predictive torque control based on a composite sliding mode disturbance observer is proposed. Firstly, the parallel structure of torque and magnetic chain is designed. The weighting factors are eliminated by choosing a common optimal voltage vector. Secondly, a composite sliding mode perturbation observer is designed to reduce the dependence on an accurate model of the motor. An improved variable gain approximation rate is introduced to eliminate observer jitter. A power exponential term is added to improve the exponential approximation term and increase the convergence speed of the system state. Finally, the experimental results show that the proposed strategy not only eliminates the cumbersome tuning work of the weight coefficients but also improves the control performance of the motor under parameter mismatch.

1. INTRODUCTION

Permanent magnet synchronous motors (PMSMs) are extensively applied in industrial production, aerospace, and other utilizations because of their great efficiency, small size, and power density [1]. The control methods primarily include field-oriented control (FOC) and direct torque control (DTC) [2]. FOC selects voltage vectors according to torque and magnetic chain errors through a pre-given switching table, which is a simple control method but has limited optional voltage vectors, resulting in large torque and magnetic chain pulsations [3]. To address the issue of large magnetic chain and torque pulsation in DTC, scholars have tried to introduce model predictive control (MPC) into DTC and achieved some success. MPC is generally used in power electronics which can be separated into continuous control set MPC and finite control set MPC (FCS-MPC) [4]. In PMSM drive system, FCS-MPC methods can be categorized into model predictive current control and model predictive torque control (MPTC) based on different control objectives [5].

MPTC performance is closely related to motor parameters and weighting factors (WF). When the actual parameters of the motor are affected by temperature rise, magnetic field saturation, and improperly selected weighting coefficients, the PMSM torque and chain prediction models produce errors, which deteriorate the control performance [6, 7]. To address the above problems, scholars have done a lot of research and proposed various solutions.

To address the problem that the prediction model of MPTC is affected by the accuracy of weighting factors, scholars have conducted the following studies. In [8], a torque and flux predictive control of an induction machine drive fed by a three-phase two-level voltage source inverter is proposed. The strategy replaces a single cost function with a multi-objective optimization based on a ranking method. This method does not require adjustment of the weighting factors, but it is difficult to achieve global optimization in terms of the total harmonic distortion of the current. In [9], a numerical WF processing strategy based on state normalization and variable sensitivity balancing is proposed. The method simplifies the construction of the objective function and the correction of the weighting coefficients, but the model's generality is limited, making it hard to adapt to diverse system structures and parameters. In [10], an AC motor torque and flux control strategy is proposed. The method is based on MPC using one cost function for torque and a separate cost function for flux control. This avoids the need to design weight coefficients. However, the dual cost function architecture makes the algorithm more complex and increases the computational load, which affects the real-time performance of the system. In [11], a direct voltage-vector selection-based model-predictive direct-speed control method is proposed. The method constructs a cost function by utilizing this reference voltage vector. The design of weighting coefficients is avoided, but this direct voltage vector selection method limits the system's dynamic response performance in complex operating conditions and reduces real-time calculation efficiency. In [12], an improved unweighted coefficient predictive torque control method is proposed. The method constructs a cost function based on the stator chain vector tracking error to avoid WF design, but this method needs really accurate real-time measurements of the stator chain vector. In [13], a chaotic variant-based dynamic reorganization multiple swarm particle swarm algorithm realizing self-tuning of weighting coefficients

* Corresponding author: Zhun Cheng (120277982@qq.com).

is proposed. This method realizes the self-adjustment of weight coefficients, but the frequent switching of operating states may lead to unstable PMSM control performance.

To address the issue that the control effect of MPTC is affected by the accuracy of motor parameters, scholars have conducted the following studies. In [14], an improved deadbeat (DB) predictive current control based on multi-parameter identification is proposed. The scheme effectively solves the coupling problem in multi-parameter identification by constructing a current prediction error model. The ability of motor parameter identification is improved. However, the calculation is large. In [15], a parameter identification method for obtaining important motor parameters such as flux and inductance using online particle swarm optimization is proposed. The proposed method can identify both stator inductance and magnetic flux, but the complexity of the algorithm is high. In [16], a sliding mode observer based mechanical parameter estimation algorithm for permanent magnet synchronous motor drive system is proposed. The smoothed output of the observer can be directly used for parameter estimation, but this algorithm is super dependent on how the sliding surface is designed, and if it is not done right, it can mess up how well the observer works. In [17], a model predictive current control based on sliding mode observer is proposed. The sliding mode disturbance observer designed by this method can compensate and predict lumped disturbances such as parameter mismatch and unmodeled dynamic disturbances in the model, but the parameters of the observer are difficult to be designed. In [18], an improved DB prediction controller for PMSM drive systems is proposed. It can eliminate the effects of parameter mismatches such as inductance, resistance, and flux linkage. However, the design of the controller parameters relies on experience. In [19], a novel technique based on a sliding mode perturbation observer is proposed. The method eliminates internal PMSM demagnetization faults affected by stator parameter mismatch, but there is a certain delay. In [20], a fractional-order sliding mode control strategy based on higher-order nonlinear disturbance observers is proposed. The proposed method can estimate the matching perturbation and mismatch perturbation. However, the stator current harmonics may be distorted.

To deal with the problem of MPTC control performance in PMSM which is subject to weighted realignment and motor parameters, a no weighing factor model predictive torque control based on a composite sliding mode disturbance observer (CSMDO-NWFMPTC) is proposed. Compared with the conventional MPTC, it omits the design of WF and improves the control performance of the motor under parameter mismatch. When the motor parameters are changed, the method still obtains better control performance. The major contributions of this paper are as follows:

1) The proposed no weighting factors model predictive torque control (NWFMPTC) eliminates the cumbersome weight factor adjustment process in traditional methods by selecting a common optimized voltage vector through the design of a parallel structure between torque and flux linkage.

2) The proposed CSMDO-NWFMPTC design employs a composite sliding mode disturbance observer (CSMDO). By introducing improved variable gain approximation rate and power index terms, observer chatter is effectively suppressed, disturbance estimation accuracy improved, and system convergence speed enhanced. This improves the control performance of the motor when parameters are mismatched.

The rest of the paper is organized as follows. Section 2 introduces the mathematical model of PMSM. Section 3 introduces the fundamentals of MPTC and the sliding mode disturbance observer (SMDO). Section 4 introduces the basic principles of CSMDO-NWFMPTC. Section 5 introduces the experimental validation and simulation analysis. Finally, Section 6 briefly summarizes the paper.

2. MATHEMATICAL MODEL OF PMSM

In this paper, surface-mounted PMSM is studied, and the voltage and magnet flux linkage equations in the two-phase rotating *dq* coordinates system are as follows:

$$\begin{cases} u_d = R_s i_d + \frac{d\psi_d}{dt} - \omega_e \psi_q \\ u_q = R_s i_q + \frac{d\psi_q}{dt} + \omega_e \psi_d \end{cases} \tag{1}$$

$$\begin{cases} \psi_d = L_s i_d + \psi_f \\ \psi_q = L_s i_q \end{cases} \tag{2}$$

The electromagnetic torque equation is as follows:

$$T_e = \frac{3}{2} p \psi_f i_q \tag{3}$$

where u_d, u_q are the *dq*-axis components of stator voltage vector; i_d, i_q are the *dq*-axis components of stator current vector; ψ_d, ψ_q, and ψ_f are the *dq*-axis components of the stator and the rotor magnetic flux linkage vector; R_s and L_s are stator resistance and stator inductance; and ω_e is the rotor angular velocity of the motor.

The MPTC is constructed based on a mathematical model of the PMSM, which describes the time-domain relationships of stator voltage, magnetic chain, and torque through mathematical modeling. The model is usually calculated iteratively using the Eulerian method for the discretized state equations to predict the torque and chain values at future moments. The prediction equations for current, torque, and magnetic chain are shown as follows.

The prediction model for the current is as follows:

$$\begin{cases} i_d(k+1) = i_d(k) - \frac{R_s T_s}{L_s} i_d(k) + T_s \omega_e i_q(k) + \frac{T_s}{L_s} u_d(k) \\ i_q(k+1) = i_q(k) - \frac{R_s T_s}{L_s} i_q(k) + T_s \omega_e i_d(k) \\ \qquad - \frac{T_s}{L_s} \psi_f \omega_e(k) + \frac{T_s}{L_s} u_q(k) \end{cases} \tag{4}$$

The prediction model for the torque is as follows:

$$T_e(k+1) = \frac{3}{2} p \psi_f i_q(k+1) \tag{5}$$

The prediction model for the magnetic chain is as follows:

$$|\psi_s(k+1)| = \sqrt{(L_s i_d(k+1) + \psi_f)^2 + (L_s i_q(k+1))^2} \tag{6}$$

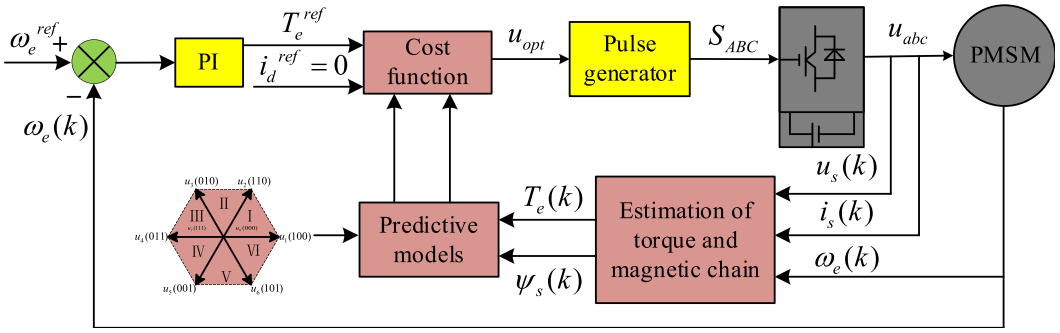

FIGURE 1. The schematic diagram of MPTC.

where $x(k)$ represents the value of x at the current moment, and $x(k+1)$ represents the predicted value of x at the next moment. x can represent current, torque, and magnetic chain.

3. THE BASIC PRINCIPLE OF MPTC AND SMDO

3.1. The Basic Concept of Weighting Factors in MPTC

The schematic block diagram of MPTC is shown in Fig. 1. The steps are as follows: First, the seven fundamental voltage vectors are brought into (4) to derive the predicted values of current after one control cycle T_s for each fundamental voltage vector. Based on the predicted values, the predicted values of torque and magnetic chain are derived. Next, the predicted values are substituted into the cost function, and the voltage vector with the smallest cost function is taken as the optimal voltage vector. Finally, the switching state corresponding to the optimal voltage vector is applied to the inverter to generate symmetrical three-phase currents to control the PMSM.

The MPTC takes the optimization of the torque and magnetic chain as the control objective, and since the two have different magnitudes it is often necessary to add a weighting factor before the magnetic chain error when setting the cost function.

$$g = \left|T_e^{ref} - T_e(k+1)\right| + \lambda \left|\psi_s^{ref} - |\psi_s(k+1)|\right| \quad (7)$$

where T_e^{ref} represents the reference value of the electromagnetic torque, ψ_s^{ref} the reference value of the stator magnetic chain, and λ the weighting factor, which is usually set empirically.

In the model predictive torque control architecture of a permanent magnet synchronous motor, the speed reference value ω_e^{ref} is input into a proportional-integral (PI) controller, which calculates it and outputs the torque reference value T_e^{ref}. Since the motor's actual operating speed dynamically changes due to load variations, speed regulation requirements, and other operational conditions, the torque reference value T_e^{ref} must be adjusted in real-time to align with the precise control objectives under different operational conditions. Therefore, the torque reference value T_e^{ref}, as the output of the PI controller, exhibits time-varying characteristics.

There are many ways to set the weight factor such as fixed weight method, dynamic adjustment method, and no weighing method. Each method has its own advantages and disadvantages, and the commonly used method is fixed weight method. Fixed-weight method is based on empirical settings, which is simple and easy to implement, but the dynamic adjustment is poor and only applicable to systems with small parameter changes and steady state conditions [21, 22]. Dynamic regulation method is highly adaptable and is often applied in situations such as sudden load changes and variable speeds, but it requires a huge amount of computational resources.

Comparative analysis shows that no weighting factors method is more suitable for the improvement of motor control performance. Therefore, from this perspective, this paper investigates how to eliminate the weighting coefficients of torque and magnetic chain by mathematical derivation. This in turn improves the control performance of the motor in high-precision and low-pulsation occasions.

3.2. The Basic Concept of SMDO

Sliding mode control belongs to an important control method in the theory of variable structure control. Its core feature is that the control law has discontinuity. Compared with the traditional continuous control method, this characteristic makes the system structure switch with the time evolution. When certain conditions are met, the state of the motor system will generate high-frequency, small-amplitude oscillations along the vicinity of a preset trajectory. This motion can be engineered independent of the parameters and perturbations of the system.

By introducing sliding mode control into the observer, one obtains SMDO. It is a nonlinear observer combining sliding mode control theory and disturbance estimation technique [23]. The core principle lies in the design of a sliding mode surface and disturbance compensation mechanism to realize the real-time estimation and dynamic suppression of the disturbance of the motor system.

SMDO consists of three basic links, which are categorized into the design of sliding mode observer, the reconstruction and compensation of perturbations, and the dynamic adjustment of the jitter. These three basic links are described as follows:

1) The design of sliding mode observer: It is the core of SMDO, which is designed to control the target by designing a sliding mold surface to make the state of the system slide along the sliding mold surface.

2) The reconstruction and compensation of perturbations: There are few PMSM systems that are free of perturbations.

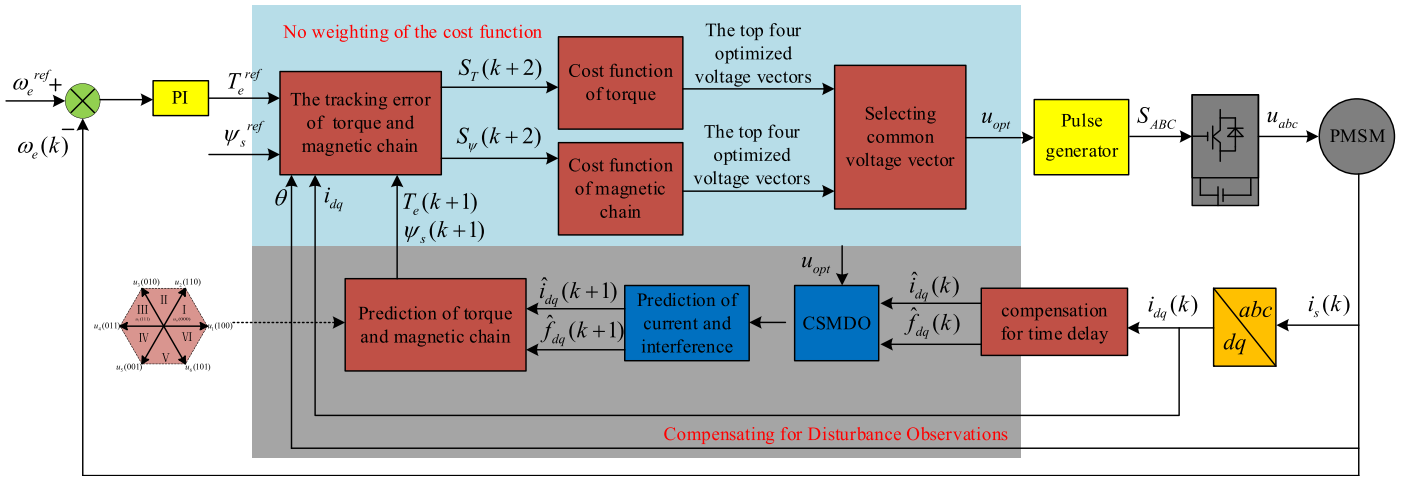

FIGURE 2. The schematic diagram of CSMDO-NWFMPTC.

In order to minimize the effects of its own parameters and the external environment on the system, they often need to be considered perturbations. Therefore, through means such as reconfiguration and compensation, the impact of disturbances on system control performance can be effectively reduced.

3) The dynamic adjustment of the jitter: The design of the convergence rate in the design of the sliding mold surface includes the jitter phenomenon caused by the high and flat switching. So in order to avoid the increase of state estimation error and the decrease of motor efficiency caused by this phenomenon, it is often necessary to dynamically adjust and compensate for the jitter.

4. THE BASIC PRINCIPLE OF CSMDO-NWFMPTC

The control block diagram of the proposed composite sliding mode disturbance observer based no weighting factor MPTC (CSMDO-NWFMPTC) strategy is shown in Fig. 2. It firstly utilizes a composite sliding mode disturbance observer to accurately estimate parameter variations and other external disturbances, and compensates them to the control system in real time. The accuracy of the system motor prediction model under parameter mismatch is improved. Then, the traditional cost function with weighting factors is transformed into an unweighted factor form with stepwise evaluation in MPTC. The electromagnetic torque and stator chain errors are evaluated separately in turn, reducing the computational effort and avoiding complex weighting factor design. Finally, the voltage vector that minimizes the torque and chain error is selected to act on the motor based on the real-time calculation of the prediction model. The control accuracy and control performance are improved.

4.1. The Design of No Weighing Factor Model Predictive Torque Control

As can be seen from (5), (6), and (7), in a conventional MPTC, the determination of the cost function allows the pulsation amplitudes of the electromagnetic torque and stator flux to track their respective reference values. However, when the ambient temperature causes the motor parameters to change, the originally fixed weight coefficients will lead to an improper selection of voltage vectors and deterioration of system control performance. To address this problem, a no weighting factor model predictive torque control (NWFMPTC) strategy is proposed to eliminate the influence of weighting factor (WF) design on motor performance.

The NWFMPTC strategy sets an improved cost function. It not only tracks the error at the current moment but also integrates the accumulated error in the past. The expressions for the proportional integral form of the tracking errors of the torque and the magnetic chain are as follows:

$$\begin{cases} S_T = e_T(t) + K_T \int_0^t e_T(\tau)dt + e_T(0) \\ S_\psi = e_\psi(t) + K_\psi \int_0^t e_\psi(\tau)dt + e_\psi(0) \end{cases} \tag{8}$$

where $e_T(t) = T_e^{ref} - T_e(t)$ and $e_\psi(t) = \psi_s^{ref} - \psi_s(t)$ are the tracking errors of the torque and magnetic chain; K_T and K_ψ are the gain coefficients of the torque and the magnetic chain.

The system is stabilized when the torque and magnetic chain follow the corresponding given values, and the tracking errors of the torque and magnetic chain satisfy the following equation.

$$\begin{cases} S_T = \frac{dS_T}{dt} = 0 \\ S_\psi = \frac{dS_\psi}{dt} = 0 \end{cases} \tag{9}$$

To perform the error accumulation correctly and rationally, the torque and chain tracking errors are updated according to the torque and chain errors at the next moment. The updated (9) is introduced into the MPTC so that the torque and magnetic chain at the next moment can accurately track their corresponding given values thus improving the robustness of the parameters. From that point of view, it is first necessary to design an appropriate cost function, because the setting of the cost function has a great influence on the performance of motor control. Introducing the proportional-integral link into the cost function

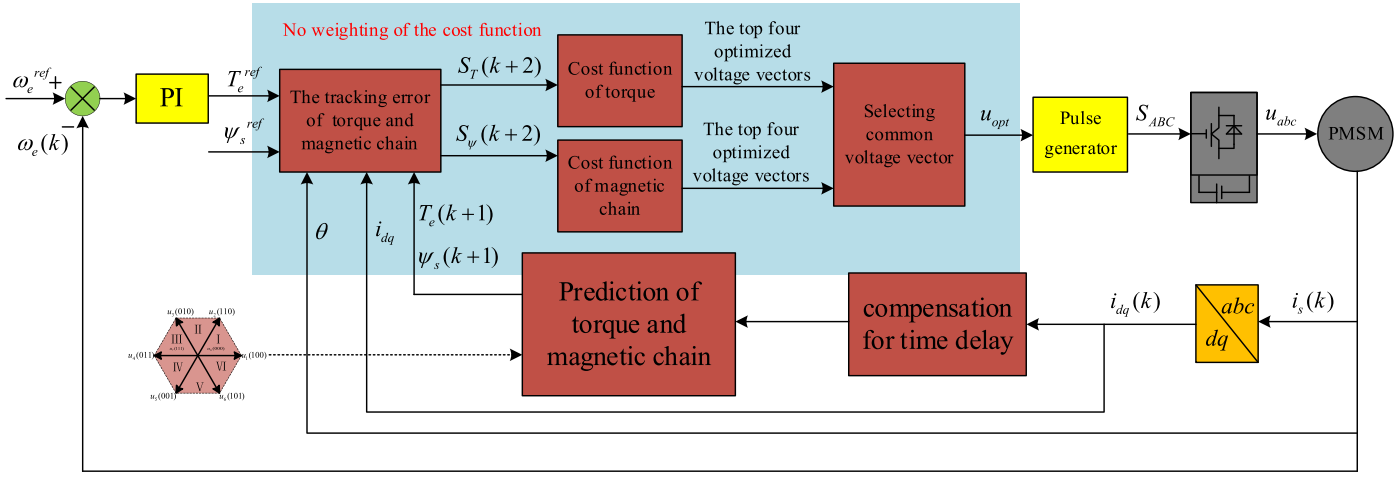

FIGURE 3. The schematic diagram of NWFMPTC.

can integrate the past cumulative error arrivals to ensure the stability of the proposed strategy. The equation is as follows:

$$\begin{cases} S_T(k) = S_T(k-1) - (e_T(k) - e_T(k-1)) \\ \qquad +K_T e_T(k) T_s \\ S_\psi(k) = S_\psi(k-1) - (e_\psi(k) - e_\psi(k-1)) \\ \qquad +K_\psi e_\psi(k) T_s \end{cases} \tag{10}$$

Combine (10) while considering the effect of delay. The proportional integral form of the tracking error can be expressed in the following equation:

$$\begin{cases} S_T(k+2) = S_T(k+1) + (e_T(k+2) - e_T(k+1)) \\ \qquad +K_T e_T(k+2) T_s \\ S_\psi(k+2) = S_\psi(k+1) + (e_\psi(k+2) - e_\psi(k+1)) \\ \qquad +K_\psi e_\psi(k+2) T_s \end{cases} \tag{11}$$

Therefore, the cost function can be expressed as follows:

$$g = |S_T(k+2)| + \lambda |S_\psi(k+2)| \tag{12}$$

To analyze the improved robustness of the proposed strategy, (12) is updated as follows:

$$g = g_T(k) + g_\psi(k) = \left| T_e^{ref} - T_e(k+2) + K_T T_s \sum_{i=1}^{k+2} e_T(i) \right|$$

$$+\lambda \left| \psi_s^{ref} - \psi_s(k+2) + K_\psi T_s \sum_{i=1}^{k+2} e_T(i) \right| \tag{13}$$

The torque and magnetic chain in the cost function are defined as follows:

$$\begin{cases} g_T(k) = \tilde{T}_e(k+2) - T_e(k+2) \\ g_\psi(k) = \tilde{\psi}_s(k+2) - T_e(k+2) \end{cases} \tag{14}$$

where $\tilde{T}_e(k+2)$ and $\tilde{\psi}_s(k+2)$ are the exact torque and chain predictions at moment $k+2$.

Each of the candidate voltage-voltage vectors has a corresponding $g_T(k)$ and $g_\psi(k)$. K_T and K_ψ can be set to compensate the accumulated error. Combining (11) with (12), the cost function of the proposed strategy can be designed as follows:

$$g = \left| T_e^{ref} - T_e(k+2) + g_T(k) + K_T T_s \sum_{i=1}^{k+2} e_T(i) \right|$$

$$+\lambda \left| \psi_s^{ref} - \psi_s(k+2) + g_\psi(k) + K_\psi T_s \sum_{i=1}^{k+2} e_T(i) \right| \tag{15}$$

For avoiding the cumbersome design of the weighting coefficients, the cost function is one part in two and expressed as follows:

$$g = g_1 + g_2 = |S_T(k+2)| + |S_\psi(k+2)| \tag{16}$$

The torque term cost function g_1 and chain term cost function g_2 in Eq. (16) both use eight voltage vectors for optimization. First, the voltage vectors are brought into g_1. Then they are sorted in ascending order, and the top four are named as torque-voltage vector group. Similarly, the voltage vectors are brought into g_2. Then, they are sorted in ascending order, and the top four are named as chain voltage vector groups. The common voltage vector of the torque vector group and voltage vector group is the optimal voltage vector, and the optimal voltage vector selected in this way is one of the first four voltage vectors in the two groups. So this method minimizes the cost function while eliminating the need to use weighting coefficients. The control block diagram of the proposed strategy is shown in Fig. 3.

4.2. The Design of a Composite Sliding Mode Disturbance Observer

SMDO is effective in estimating and suppressing disturbances in a motor control system, but its inherent jitter phenomenon leads to large fluctuations in the observation results. The accuracy is insufficient, and the robustness is reduced when facing complex, multi-source disturbances and parameter variations.

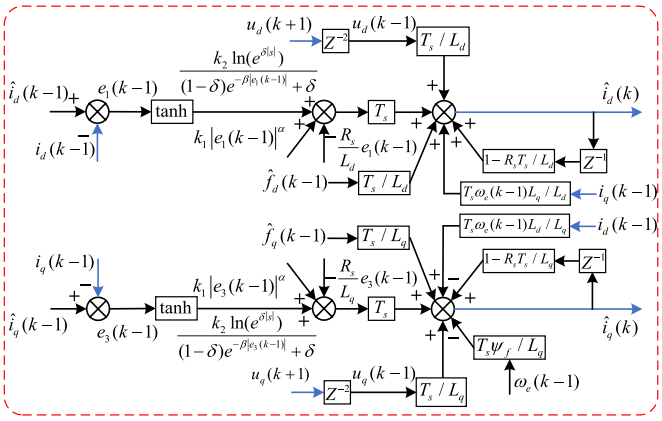

FIGURE 4. The schematic diagram of CSMDO.

Thus, to further improve the accuracy and stability of perturbation observation, a composite disturbance sliding mode observer (CSMDO) is proposed in this section to mitigate the jitter effect and enhance the system integrated suppression capability for multiple perturbations. The control block diagram of the CSMDO is shown in Fig. 4.

Considering the variation of motor parameters, the voltage equation is rewritten according to (4) as follows:

$$\begin{cases} u_d = R_s i_d + L_s \frac{di_d}{dt} - L_s \omega_e i_q + f_d \\ \frac{df_d}{dt} = F_d \end{cases} \tag{17}$$

$$\begin{cases} u_q = R_s i_q + L_s \frac{di_q}{dt} + \omega_e L_s i_d + \psi_f \omega_e + f_q \\ \frac{df_q}{dt} = F_q \end{cases} \tag{18}$$

where f_d and f_q denote the disturbances caused by parameter mismatches, which vary with a value of rate zero.

When a mismatch occurs in the motor parameters, the parameter perturbation term is shown as follows:

$$\begin{cases} f_d = \Delta \tilde{L}_s \frac{di_d}{dt} + \Delta \tilde{R} s i_d - \Delta \tilde{L}_s \omega_e i_q \\ f_q = \Delta \tilde{L}_s \frac{di_q}{dt} + \Delta \tilde{R} s i_q + \Delta \tilde{L}_s \omega_e i_d + \Delta \tilde{\psi}_f \omega_e \end{cases} \tag{19}$$

Because the observer is designed to estimate the total perturbation of the stator current and parameter set, the combination of (17) and (18) allows it to be designed as follows:

$$\begin{cases} u_d = R_s \hat{i}_d + L_d \frac{d\hat{i}_d}{dt} - L_s \omega_e i_q + \hat{f}_d + U_{ds} \\ \frac{d\hat{f}_d}{dt} = g_d U_{ds} \\ u_q = R_s \hat{i}_q + L_q \frac{d\hat{i}_q}{dt} + \omega_e L_s i_d + \psi_f \omega_e + \hat{f}_q + U_{qs} \\ \frac{d\hat{f}_q}{dt} = g_q U_{qs} \end{cases} \tag{20}$$

where $\hat{f}_d$, $\hat{f}_q$, $\hat{i}_d$, $\hat{i}_q$ denote the estimated values. g_d, g_q denote the control coefficients of the sliding mode observer. U_{ds}, U_{qs} denote the corresponding control functions.

Combining (19) and (20), the error equation can be expressed as follows:

$$\begin{cases} \frac{de_1}{dt} = -\frac{-R_s}{L_s} e_1 + \frac{1}{L_s} e_2 + \frac{1}{L_s} U_{ds} \\ \frac{de_2}{dt} = g_d U_{ds} - F_d \\ \frac{de_3}{dt} = -\frac{-R_s}{L_s} e_3 + \frac{1}{L_s} e_4 + \frac{1}{L_s} U_{qs} \\ \frac{de_4}{dt} = g_d U_{qs} - F_q \end{cases} \tag{21}$$

where e_1 and e_3 denote the estimation error of the current, and e_2 and e_4 denote the estimation error of the disturbance term.

The sliding mode control theory is designed based on surfaces and control functions. It can adjust the input signals of the control system to make the trajectory of the system to converge to the selected sliding mode surface quickly and stably. The selected sliding mode surface is shown below:

$$\begin{cases} s_d = e_1 = \hat{i}_d - i_d \\ s_q = e_3 = \hat{i}_q - i_q \end{cases} \tag{22}$$

The observation accuracy depends on the design of the convergence rate. In this case, the exponential convergence method is realized by adjusting the rate of state change of the motor drive system. It is formulated as follows:

$$\frac{ds}{dt} = -k_1^e s - k_2^e \operatorname{sgn}(s) \tag{23}$$

However in the exponential convergence method, there is an increase in observer jitter due to fixed gain. Therefore to solve this problem, the new exponential convergence method is improved as follows:

$$\frac{ds}{dt} = -k_1^e |s|^\alpha - \frac{k_2 \mathrm{In}\left(e^{\delta|s|}\right)}{(1-\delta)e^{-\beta|s|} + \delta} \operatorname{sgn}(s) \tag{24}$$

where $k_1 > 1$, $k_2 > 0$, $0 < \alpha < 1$, $\beta > 1$, $0 < \delta < 1$.

When the motor operates normally, its trajectory is close to the surface of the slide mold. The gain term $k_2 \mathrm{In}(e^{\delta|s|}) / \left[(1-\delta)e^{-\beta|s|} + \delta\right]$ converges to 0, and the jitter of the system observer is suppressed. The approximate speed of the motor system is further enhanced as the trajectory moves away from the surface, and the variable gain term tends to infinity. The exponential convergence rate is accelerated by adding an exponential power term $|s|^\alpha$, thereby improving the system's convergence behaviour.

In order to ensure the estimation accuracy of errors e_1, e_3 and disturbance estimation errors e_2, e_4, a Lyapunov function is introduced to verify the stability of the system and improved convergence rate, as shown below:

$$V = \frac{1}{2} s^2 \tag{25}$$

The first order differential equation of the above equation can be expressed as follows:

$$\frac{dV}{dt} = s \frac{ds}{dt} = -k_1 s |s|^\alpha$$

$$-\frac{sk_2\mathrm{In}\left(e^{\delta|s|}\right)}{(1-\delta)e^{-\beta|s|}+\delta}\,\mathrm{sgn}(s)\frac{dy}{dx}\le 0 \tag{26}$$

When parameters $k_1>0$, $k_2>0$, $\beta>0$, $0<\alpha<1$, $0<\delta<1$, the convergence of the exponential convergence method satisfies the stability condition.

The substitution of (22) into (24) yields:

$$\begin{cases}\frac{de_1}{dt}=-k_1\left|e_1\right|^{\alpha}-\frac{k_2\mathrm{In}\left(e^{\delta|s|}\right)}{(1-\delta)e^{-\beta|e_1|}+\delta}\,\mathrm{sgn}(e_1)\\ \frac{de_3}{dt}=-k_1\left|e_3\right|^{\alpha}-\frac{k_2\mathrm{In}\left(e^{\delta|s|}\right)}{(1-\delta)e^{-\beta|e_3|}+\delta}\,\mathrm{sgn}(e_3)\end{cases} \tag{27}$$

Taking e_2 and e_4 as disturbance values. The control function function is designed as follows:

$$\begin{cases}U_{ds}=L_s\left[k_1\left|e_1\right|^{\alpha}+\frac{k_2\mathrm{In}\left(e^{\delta|s|}\right)}{(1-\delta)e^{-\beta|s|}+\delta}\,\mathrm{sgn}(e_1)\right]-R_se_1\\ U_{qs}=L_s\left[k_1\left|e_3\right|^{\alpha}+\frac{k_2\mathrm{In}\left(e^{\delta|s|}\right)}{(1-\delta)e^{-\beta|s|}+\delta}\,\mathrm{sgn}(e_3)\right]-R_se_3\end{cases} \tag{28}$$

The current estimation error is needed to ensure that the motor is in a converged state during its operation. To fulfill the above conditions, the observer is set up as follows:

$$\begin{cases}\frac{dV_d}{dt}=s_d\frac{ds_d}{dt}\le 0\\ \frac{dV_q}{dt}=s_q\frac{ds_q}{dt}\le 0\end{cases} \tag{29}$$

Taking V_d as an example, the stability conditions are recast on the basis of the above analysis as follows:

$$\begin{aligned}\frac{dV_d}{dt}&=-\frac{1}{Ls}e_1e_2-k1e1\left|e1\right|^{\alpha}\\ &\quad-\frac{e_1k_2\mathrm{In}\left(e^{\delta|s|}\right)}{(1-\delta)e^{-\beta|s|}+\delta}\,\mathrm{sgn}(e_1)\le 0\end{aligned} \tag{30}$$

The system parameters k_1 and k_2 need to satisfy the following equations when the system is in stable operation:

$$\begin{cases}k_1>0\\ k_2>\frac{1}{L_s}\left|e_2\right|\end{cases} \tag{31}$$

So the parameters of the observer that need to be satisfied are set as follows:

$$\begin{cases}k_1>0\\ k_2>\max\left[\frac{1}{L_s}\left|e_2\right|,\frac{1}{L_s}\left|e_4\right|\right]\end{cases} \tag{32}$$

According to the above analysis, when the optimal voltage vector applied at moment $k-1$ is a zero vector, the perturbation value calculated from sampling at moment k is directly related to the current error. On this basis, the discrete form equation of the composite observer is shown below:

$$\begin{cases}\hat{i}_d(k)=\hat{i}_d(k-1)\left[1-\frac{R_sT_s}{L_s}\right]+u_d(k-1)\frac{T_s}{L_s}\\ +i_q(k-1)T_s\omega_e(k-1)+\hat{f}_d(k-1)\frac{T_s}{L_s}+U_{ds}(k-1)\frac{T_s}{L_s}\\ \hat{i}_q(k)=\hat{i}_q(k-1)\left[1-\frac{R_sT_s}{L_s}\right]+u_q(k-1)\frac{T_s}{L_s}\\ -i_d(k-1)T_s\omega_e(k-1)-\omega_e(k-1)\frac{T_s\psi_f}{L_s}\\ +\hat{f}_q(k-1)\frac{T_s}{L_s}+U_{qs}(k-1)\frac{T_s}{L_s}\\ \hat{f}_d(k)=U_{ds}(k-1)g_dT_s+\hat{f}_d(k-1)\\ \hat{f}_d(k)=U_{qs}(k-1)g_qT_s+\hat{f}_q(k-1)\end{cases} \tag{33}$$

where $\hat{i}_d$ and $\hat{i}_q$ denote the observed values of stator current at moment k. $\hat{f}_d$ and $\hat{f}_q$ denote the observed values of parameter perturbation at moment k.

The discretized expression for the control function is shown below:

$$\begin{cases}U_{ds}(k-1)=L_sk_1\left|e_1(k-1)\right|^{\alpha}+L_s\tan h(e_1(k-1))\\ \qquad\frac{k_2\mathrm{In}\left(e^{\delta|s|}\right)}{(1-\delta)e^{-\beta|e_1(k-1)|}+\delta}-R_se_1(k-1)\\ U_{qs}(k-1)=L_sk_1\left|e_3(k-1)\right|^{\alpha}+L_s\tan h(e_1(k-1))\\ \qquad\frac{k_2\mathrm{In}\left(e^{\delta|s|}\right)}{(1-\delta)e^{-\beta|e_3(k-1)|}+\delta}-R_se_3(k-1)\end{cases} \tag{34}$$

In order to effectively reduce the predicted current ripple caused by the sign function, this section uses a smooth continuous hyperbolic tangent function instead of the sign function. A smoother transition characteristic is realized, which effectively reduces the current ripple.

The parameter perturbations in (35) are substituted into the prediction equations:

$$\begin{cases}\hat{i}_d(k+1)=\hat{i}_d(k)\left[1-\frac{R_sT_s}{L_s}\right]+u_d(k)\frac{T_s}{L_s}\\ +i_q(k)T_s\omega_e(k)+\hat{f}_d(k)\frac{T_s}{L_s}+U_{ds}(k)\frac{T_s}{L_s}\\ \hat{i}_q(k+1)=\hat{i}_q(k)\left[1-\frac{R_sT_s}{L_s}\right]+u_q(k)\frac{T_s}{L_s}\\ -i_d(k)T_s\omega_e(k)-\omega_e(k)\frac{T_s\psi_f}{L_s}\\ +\hat{f}_q(k)\frac{T_s}{L_s}+U_{qs}(k)\frac{T_s}{L_s}\\ \hat{f}_d(k+1)=U_{ds}(k)g_dT_s+\hat{f}_d(k)\\ \hat{f}_d(k+1)=U_{qs}(k)g_qT_s+\hat{f}_q(k)\end{cases} \tag{35}$$

The predicted values of stator currents and parameter perturbations are obtained through the prediction equations. Thus, the reference value of the *dq* axis of the voltage vector can be expressed as follows:

$$\begin{cases}u_d=\frac{L_s}{T_s}\left(i_d^{ref}-i_d(k-1)\left[1-\frac{R_sT_s}{L_s}\right]\right.\\ \qquad\left.-T_s\omega_e\hat{i}_d(k+1)\right)\\ u_q=\frac{L_s}{T_s}\left(i_q^{ref}-i_q(k-1)\left[1-\frac{R_sT_s}{L_s}\right]\right.\\ \qquad\left.-T_s\omega_e\hat{i}_q(k+1)+\frac{T_s\psi_f\omega_e(k)}{Ls}\right)\end{cases} \tag{36}$$

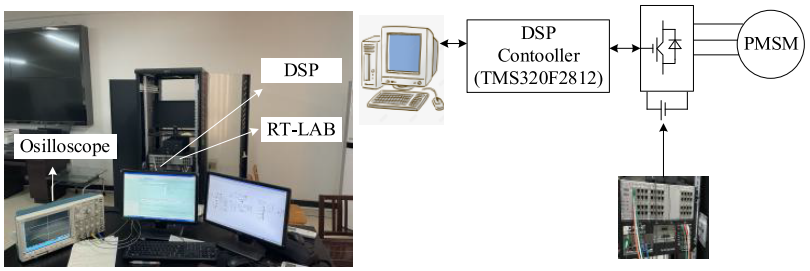

(a) (b)

FIGURE 5. (a) The diagram of RT-LAB semi-physical simulation platform. (b) The schematic diagram of the RT-LAB hardware.

Combining (35) and (36), the predicted total parameter perturbations a and b are compensated as compensation voltages into the reference voltage vector as follows:

$$\begin{cases} u_d^{com}(k+1) = \hat{f}_d(k+1) + u_d^{ref} \\ u_q^{com}(k+1) = \hat{f}_q(k+1) + u_q^{ref} \end{cases} \tag{37}$$

where u_d^{com} and u_q^{com} denote the compensated reference voltage vectors.

To address the jitter problem and insufficient multi-source disturbance suppression capability of the SMDO in the control of PMSM, the CSMDO proposed in this paper improves the performance of the system through the following steps:

1) The disturbance observation model is reconstructed based on the motor voltage equations under parameter mismatch, and the disturbance terms caused by parameter changes are included in the total disturbance estimation.

2) A new exponential convergence law with variable gain characteristics is designed to achieve jitter vibration suppression near the sliding mode surface with fast convergence away from it by introducing dynamic adjustment coefficients.

3) Ljapunov stability theory is further employed to rigorously derive the observer parameter constraints to ensure that the system is globally stable.

4) Smooth switching is achieved by replacing the traditional sign function with hyperbolic tangent function, and the complete predictive compensation control architecture is constructed by combining the discretization design. This composite design retains the strong robustness of the sliding mode control and significantly improves the control performance of the motor under system parameter mismatch through.

5. EXPERIMENTAL RESULTS AND ANALYSIS

In order to verify the correctness and effectiveness of the proposed strategy CSMDO-NWFMPTC, the simulation experiments of strategy MPTC, strategy NWFMPTC, and strategy CSMDO-NWFMPTC are carried out on an RT-LAB semi-physical simulation platform based on TMS320F2812 controller. The RT-LAB semi-physical simulation platform is shown in Fig. 5(a), the RT-LAB hardware-in-the-loop schematic shown in Fig. 5(b), and the PMSM parameters are shown in Table 1.

The experimental conditions are organized as follows

TABLE 1. The parameters of PMSM system.

Parameter	Symbol	Value
Number of pole pairs	n_p	4
Stator inductance	L_s	8.5 mH
Stator resistance	R_s	2.875 Ω
Magnet flux linkage	ψ_f	0.3 Wb
DC voltage	U_{dc}	380 V
Rated torque	T_e	12 N·m
Rated speed	N	750/min
Rated power	P_N	1 kW
Inertia	J	0.00816 kg·m^2

1) The parameter mismatch types are: 25% mismatch of the magnetic chain, 25% mismatch of the magnetic chain and inductance at the same time, 125% mismatch of the magnetic chain, and 125% mismatch of the magnetic chain and inductance at the same time.

2) The operating conditions are set as follows: the motor runs at 750 r/min; the motor speed rises to 1000 r/min in 0.3 s. Load setting: the motor runs at 7 N·m with load; the load rises to 12 N·m in 0.4 s. The motor speed is set at 1000 r/min.

5.1. The Dynamic Analysis of dq-Axis Current

Figures 6, 7, and 8 show the dq-axis current waveforms when parameter mismatch occurs in the motor for the three strategies. For ease of analysis, the dq axis current pulsation amplitudes are organized into Table 2.

The strategy NWFMPTC reduces the d-axis current pulsation value by 24.20% and the q-axis current pulsation value by 22.83% compared to the strategy MPTC. The strategy CSMDO-NWFMPTC reduces the d-axis current pulsation value by 50.49% compared to the strategy MPTC. q-axis current pulsation value is reduced by 46.38%. The dq-axis current pulsation values are shown in Table 2. It can be seen that when the motor parameters are mismatched, the strategy CSMDO-NWFMPTC reduces the dq axis current pulsation value of PMSM at MPTC.

5.2. The Dynamic Analysis of Speed and Torque

Figure 9 through Figure 11 show the speed and torque waveforms when parameter mismatch occurs in the motor for the

TABLE 2. Table of *dq* axis current pulsation amplitude.

Type of mismatch	MPTC		NWFMPTC		CSMDO-NWFMPTC	
	i_q (A)	i_d (A)	i_q (A)	i_d (A)	i_q (A)	i_d (A)
$0.75\psi_f$	1.531	2.319	1.133	1.809	0.903	1.394
$0.75L_s$, $0.75\psi_f$	1.413	3.103	1.088	2.421	0.735	1.861
$1.25\psi_f$	1.631	3.431	1.284	2.573	0.791	2.195
$1.25L_s$, $1.25\psi_f$	1.251	2.313	0.988	1.688	0.688	1.272

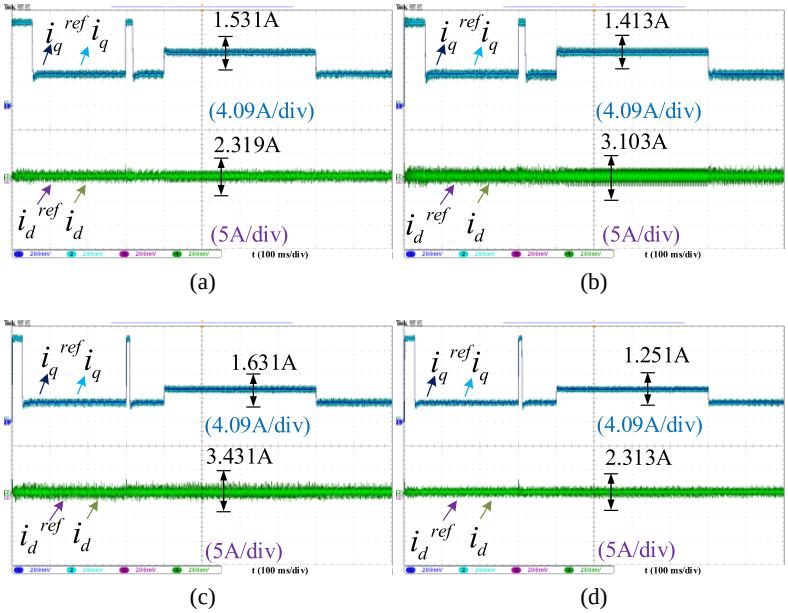

FIGURE 6. The *dq*-axis current waveform of MPTC. (a) $0.75\psi_f$, (b) $0.75L_s$, $00.75\psi_f$, (c) $1.25\psi_f$, (d) $1.25L_s$, $1.25\psi_f$.

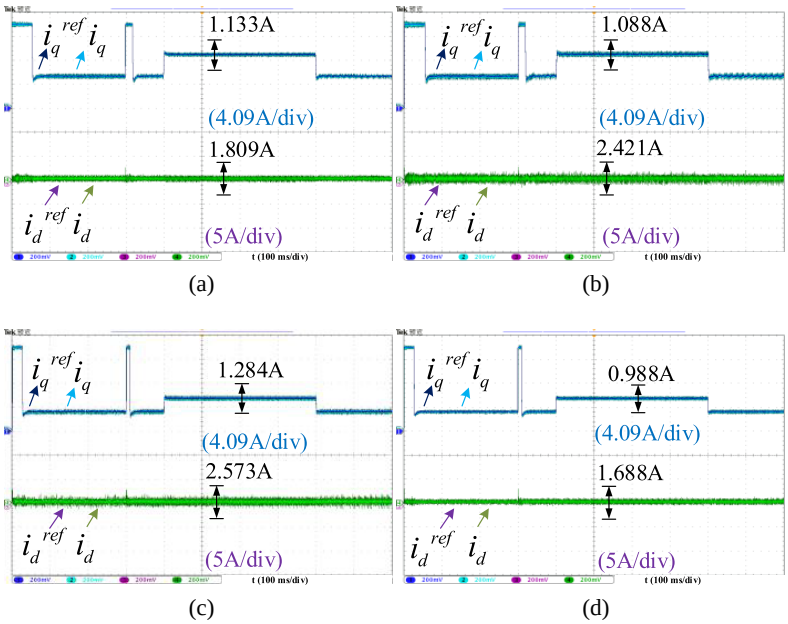

FIGURE 7. The *dq*-axis current waveform of NWFMPTC. (a) $0.75\psi_f$, (b) $0.75L_s$, $0.75\psi_f$, (c) $1.25\psi_f$, (d) $1.25L_s$, $1.25\psi_f$.

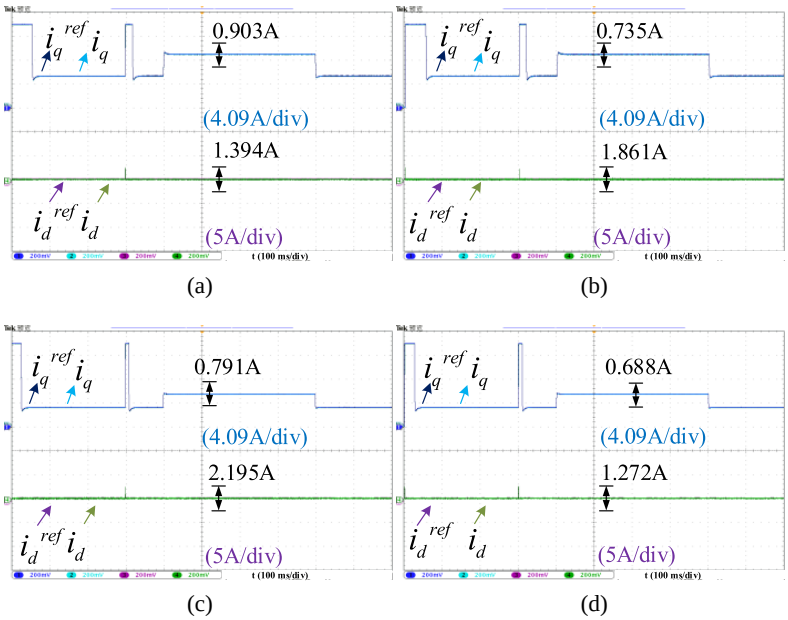

FIGURE 8. The dq-axis current waveform of CSMDO-NWFMPTC. (a) $0.75\psi_f$, (b) $0.75L_s$, $0.75\psi_f$, (c) $1.25\psi_f$, (d) $1.25L_s$, $1.25\psi_f$.

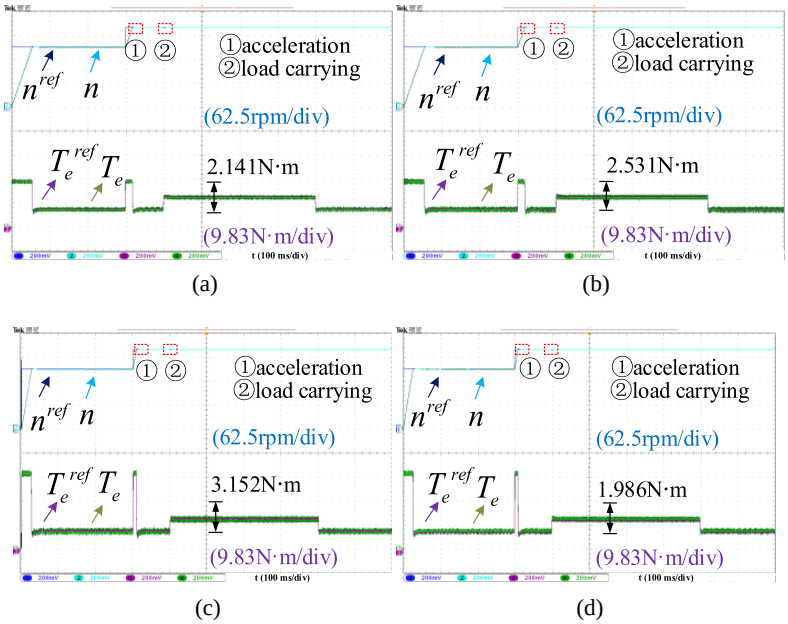

FIGURE 9. The speed and torque waveforms of MPTC. (a) $0.75\psi_f$, (b) $0.75L_s$, $0.75\psi_f$, (c) $1.25\psi_f$, (d) $1.25L_s$, $1.25\psi_f$.

TABLE 3. The speed start-up response time and torque pulsation value.

Type of mismatch	MPTC		NWFMPTC		CSMDO-NWFMPTC	
	t (s)	T_e (N·m)	t (s)	T_e (N·m)	T (s)	T_e (N·m)
$0.75\psi_f$	0.0823	2.141	0.0793	1.692	0.0764	1.392
$0.75L_s$, $0.75\psi_f$	0.0813	2.531	0.0765	1.974	0.0722	1.671
$1.25\psi_f$	0.0531	3.152	0.0529	2.522	0.0521	2.112
$1.25L_s$, $1.25\psi_f$	0.0473	1.986	0.0482	1.549	0.0431	1.311

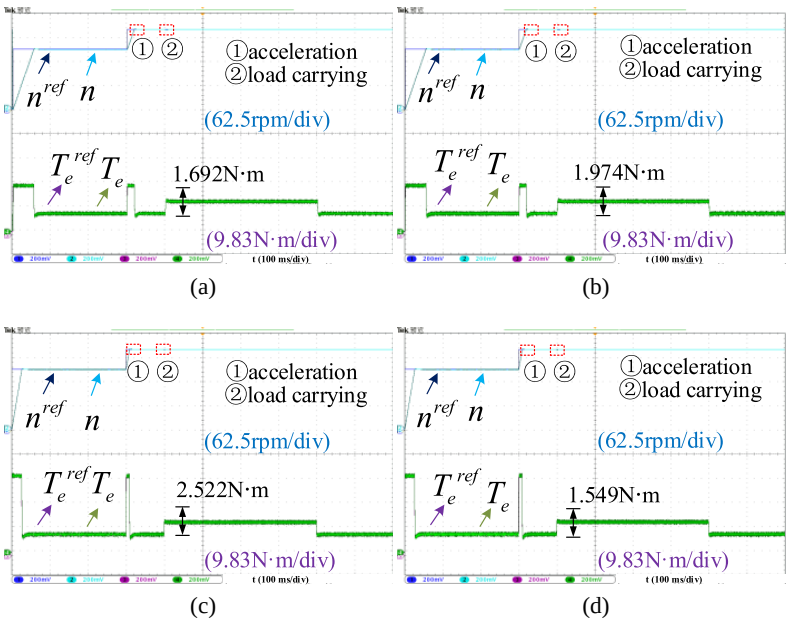

FIGURE 10. The speed and torque waveforms of NWFMPTC. (a) $0.75\psi_f$, (b) $0.75L_s$, $0.75\psi_f$, (c) $1.25\psi_f$, (d) $1.25L_s$, $1.25\psi_f$.

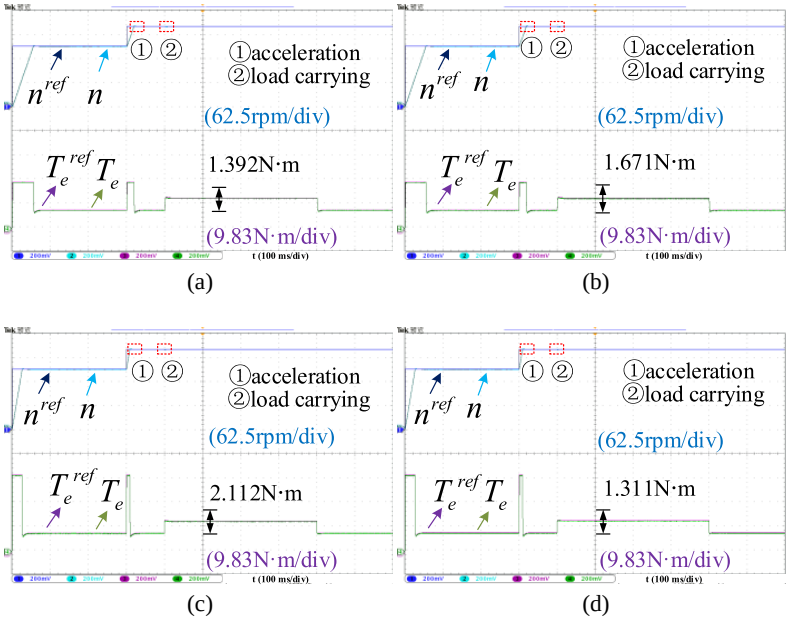

FIGURE 11. The speed and torque waveforms of CSMDO-NWFMPTC. (a) $0.75\psi_f$, (b) $0.75L_s$, $0.75\psi_f$, (c) $1.25\psi_f$, (d) $1.25L_s$, $1.25\psi_f$.

TABLE 4. The result of stator current amplitude and its THD value.

Type of mismatch	MPTC		NWFMPTC		CSMDO-NWFMPTC	
	i_a (A)	THD (%)	i_a (A)	THD (%)	i_a (A)	THD (%)
$0.75\psi_f$	18.2133	6.74	18.2126	5.39	18.2123	4.18
$0.75L_s$, $0.75\psi_f$	182142	6.91	182131	5.46	182125	4.27
$1.25\psi_f$	11.2335	6.37	11.2329	5.09	11.2326	3.94
$1.25L_s$, $1.25\psi_f$	11.2329	6.43	11.2325	5.68	11.2321	3.99

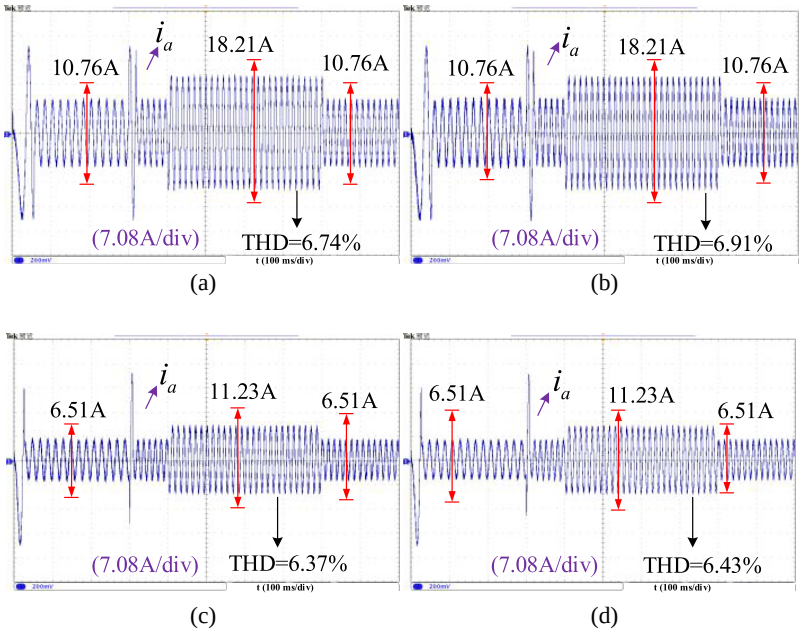

FIGURE 12. The waveform of the stator current under MPTC. (a) $0.75\psi_f$, (b) $0.75L_s$, $0.75\psi_f$, (c) $1.25\psi_f$, (d) $1.25L_s$, $1.25\psi_f$.

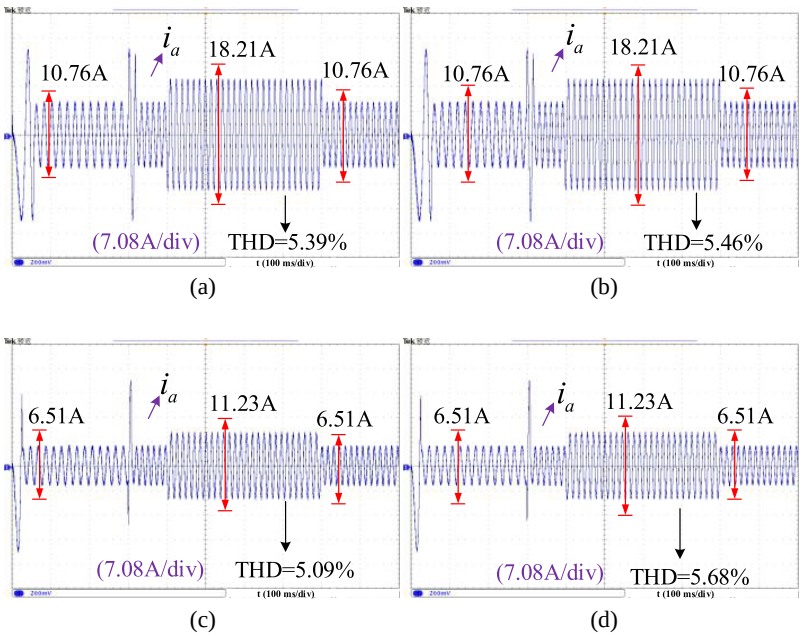

FIGURE 13. The waveform of the stator current under NWFMPTC. (a) $0.75\psi_f$, (b) $0.75L_s$, $0.75\psi_f$, (c) $1.25\psi_f$, (d) $1.25L_s$, $1.25\psi_f$.

three strategies. The speed and torque values are organized into Table 3 for ease of analysis.

The improvement of rotational speed: The response time, overshoot, and drop values of rotational speed under the three strategies are approximately the same. The electromagnetic torque improvement: the strategy NWFMPTC reduces the torque pulsation value by 21.37% compared to the strategy MPTC. The strategy CSMDO-NWFMPTC reduces the torque pulsation value by 33.98% compared to the strategy MPTC. Therefore, it can be concluded that the proposed strategy CSMDO-NWFMPTC can reduce the torque pulsation value of the motor when the PMSM is parameter mismatched.

5.3. The Dynamic Analysis of Stator Currents and Its Total Harmonic Distortion (THD)

The waveforms of stator current when parameter mismatch occurs in the motor under the three strategies are shown in Fig. 12 through Fig. 14. In order to facilitate the analysis, the relevant data are organized into Table 4.

When parameter mismatch occurs, the magnitude of the stator current i_a is approximately the same for all three strategies, with the difference being the THD value of the stator current. The strategy NWFMPTC reduces the stator current THD value by 18.19% compared to the strategy MPTC. The strat-

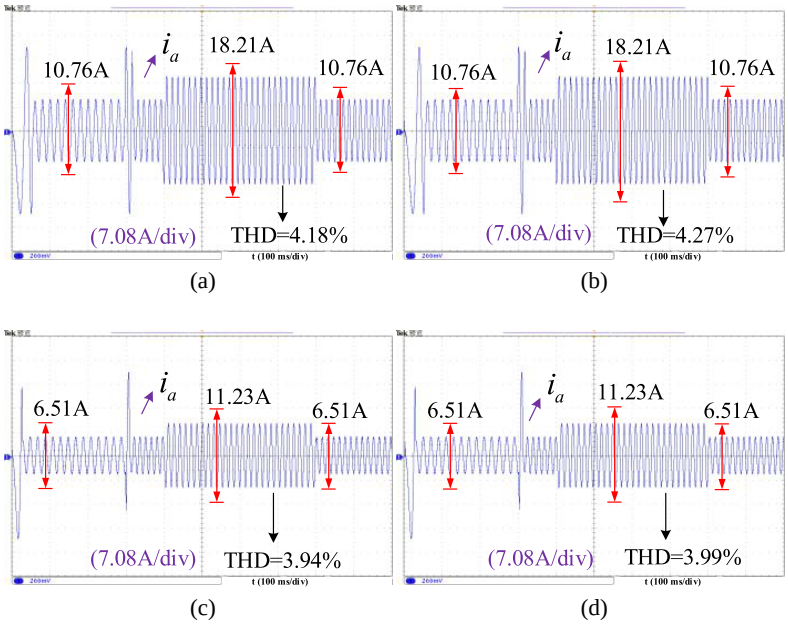

FIGURE 14. The waveform of the stator current under CSMDO-NWFMPTC. (a) $0.75\psi_f$, (b) $0.75L_s$, $0.75\psi_f$, (c) $1.25\psi_f$, (d) $1.25L_s$, $1.25\psi_f$.

egy CSMDO-NWFMPTC reduces the stator current THD by 38.07% compared to the strategy MPTC. Therefore, the proposed strategy CSMDO-NWFMPTC effectively reduces the THD value under parameter mismatch conditions.

6. CONCLUSION

To address the difficulty of adjusting weight factors and the sensitivity of control performance to motor parameters in MPTC, a no weighting factor MPTC strategy based on a composite sliding mode disturbance observer (CSMDO-NWFMPTC) is proposed. Based on the experimental results and theoretical analysis, the following conclusions can be drawn:

1) The parallel structure of torque and magnetic chain is designed in the no weighting factor MPTC (NWFMPTC) strategy. The weighting factors are eliminated by selecting the common optimal voltage vector, which avoids the cumbersome rectification of weighting factors. Compared with the conventional MPTC strategy, the d-axis current pulsation value is reduced by 24.20%, the q-axis current pulsation value reduced by 22.83%, the torque pulsation value reduced by 21.37%, and the stator current THD reduced by 18.19%.

2) A composite sliding mode disturbance observer (CSMDO) is added and designed to suppress the jitter vibration and enhance the estimation compensation capability for the disturbance. The control performance of the motor under parameter mismatch is improved. Compared to the MPTC strategy, CSMDO-NWFMPTC reduces the d-axis current pulsation value by 50.49%, the q-axis current pulsation value by 46.38%, the torque pulsation value by 33.98%, and the stator current THD by 38.07%.

ACKNOWLEDGEMENT

This work was supported by the Scientific Research Fund of Hunan Provincial Education Department under Grant Number 24A0395.

REFERENCES

[1] Zhu, L., B. Xu, and H. Zhu, "Interior permanent magnet synchronous motor dead-time compensation combined with extended Kalman and neural network bandpass filter," *Progress In Electromagnetics Research M*, Vol. 98, 193–203, 2020.

[2] Zhang, Y., S. Li, B. Luo, C. Luo, and Z. Yu, "Output current harmonic analysis and suppression method for PMSM drive system with modular multilevel converter," *IET Renewable Power Generation*, Vol. 17, No. 13, 3289–3297, Oct. 2023.

[3] Zhang, H., T. Fan, L. Meng, *et al.*, "Polynomial estimation of chain for predictive current control in PMSM," *IEEE Journal of Emerging and Selected Topics in Power Electronics*, Vol. 10, No. 5, 6112–6122, Oct. 2022.

[4] Liu, X., Y. Pan, L. Wang, J. Xu, Y. Zhu, and Z. Li, "Model predictive control of permanent magnet synchronous motor based on parameter identification and dead time compensation," *Progress In Electromagnetics Research C*, Vol. 120, 253–263, 2022.

[5] Liu, X., Y. Pan, Y. Zhu, H. Han, and L. Ji, "Decoupling control of permanent magnet synchronous motor based on parameter identification of fuzzy least square method," *Progress In Electromagnetics Research M*, Vol. 103, 49–60, 2021.

[6] Wang, Y., Y. Xu, and J. Zou, "Online multiparameter identification method for sensorless control of SPMSM," *IEEE Transactions on Power Electronics*, Vol. 35, No. 10, 10 601–10 613, Oct. 2020.

[7] Cheng, Z., C. Zhang, and Y. Zhang, "PMSWG parameter identification method based on improved operator genetic algorithm," *Progress In Electromagnetics Research C*, Vol. 139, 67–77, 2023.

[8] Rojas, C. A., J. Rodriguez, F. Villarroel, J. R. Espinoza, C. A. Silva, and M. Trincado, "Predictive torque and flux control without weighting factors," *IEEE Transactions on Industrial Electronics*, Vol. 60, No. 2, 681–690, Feb. 2013.

[9] Gong, C., Y. Hu, M. Ma, J. Gao, and K. Shen, "Novel analytical weighting factor tuning strategy based on state normalization and variable sensitivity balance for PMSM FCS-MPTC," *IEEE/ASME Transactions on Mechatronics*, Vol. 25, No. 3, 1690–1694, Jun. 2020.

[10] Norambuena, M., J. Rodriguez, Z. Zhang, F. Wang, C. Garcia, and R. Kennel, "A very simple strategy for high-quality performance of AC machines using model predictive control," *IEEE Transactions on Power Electronics*, Vol. 34, No. 1, 794–800, Jan. 2019.

[11] Zhang, X. and Y. He, "Direct voltage-selection based model predictive direct speed control for PMSM drives without weighting factor," *IEEE Transactions on Power Electronics*, Vol. 34, No. 8, 7838–7851, Aug. 2019.

[12] Xiao, M., T. Shi, Y. Yan, W. Xu, and C. Xia, "Predictive torque control of permanent magnet synchronous motors using flux vector," *IEEE Transactions on Industry Applications*, Vol. 54, No. 5, 4437–4446, Sep.-Oct. 2018.

[13] Li, J., F. Wang, D. Ke, Z. Li, and L. He, "Weighting factors design of model predictive control for permanent magnet synchronous machine using particle swarm optimization," *Transactions of China Electrotechnical Society*, Vol. 36, No. 3, 50–59, Jan. 2021.

[14] Wang, L., S. Zhang, C. Zhang, and Y. Zhou, "An improved deadbeat predictive current control based on parameter identification for PMSM," *IEEE Transactions on Transportation Electrification*, Vol. 10, No. 2, 2740–2753, Jun. 2024.

[15] Xie, C., S. Zhang, X. Li, Y. Zhou, and Y. Dong, "Parameter identification for SPMSM with deadbeat predictive current control using online PSO," *IEEE Transactions on Transportation Electrification*, Vol. 10, No. 2, 4055–4064, Jun. 2024.

[16] Zhang, X. and Z. Li, "Sliding-mode observer-based mechanical parameter estimation for permanent magnet synchronous motor," *IEEE Transactions on Power Electronics*, Vol. 31, No. 8, 5732–5745, Aug. 2016.

[17] Xu, Y., Z. Yan, Y. Zhang, and R. Song, "Model predictive current control of permanent magnet synchronous motor based on sliding mode observer with enhanced current and speed tracking ability under disturbance," *IEEE Transactions on Energy Conversion*, Vol. 38, No. 2, 948–958, Jun. 2023.

[18] Sun, X., J. Cao, G. Lei, Y. Guo, and J. Zhu, "A robust deadbeat predictive controller with delay compensation based on composite sliding-mode observer for PMSMs," *IEEE Transactions on Power Electronics*, Vol. 36, No. 9, 10 742–10 752, Sep. 2021.

[19] Han, Y., S. Chen, C. Gong, X. Zhao, F. Zhang, and Y. Li, "Accurate SM disturbance observer-based demagnetization fault diagnosis with parameter mismatch impacts eliminated for IPM motors," *IEEE Transactions on Power Electronics*, Vol. 38, No. 5, 5706–5710, May 2023.

[20] Lin, X., J. Liu, F. Liu, Z. Liu, Y. Gao, and G. Sun, "Fractional-order sliding mode approach of buck converters with mismatched disturbances," *IEEE Transactions on Circuits and Systems I: Regular Papers*, Vol. 68, No. 9, 3890–3900, Sep. 2021.

[21] Zerdali, E., M. Rivera, and P. Wheeler, "A review on weighting factor design of finite control set model predictive control strategies for AC electric drives," *IEEE Transactions on Power Electronics*, Vol. 39, No. 8, 9967–9981, Aug. 2024.

[22] Xu, S., C. Yao, G. Ren, Z. Sun, S. Wu, and G. Ma, "Weighting factors auto-tuning of FCS-MPC for hybrid ANPC inverter in PMSM drives based on deep residual networks," *IEEE Transactions on Power Electronics*, Vol. 39, No. 12, 16 540–16 552, Dec. 2024.

[23] He, L., F. Wang, W. Tian, J. Rodríguez, and M. L. Heldwein, "Predefined-time sliding mode predictive current control for disturbance suppression and dynamic response improvement in SPMSM drives," *IEEE Transactions on Industrial Electronics*, Vol. 72, No. 2, 1292–1302, Feb. 2025.